Theoretical and Applied Fracture Mechanics 117 (2022) 103189

Contents lists available at ScienceDirect

Theoretical and Applied Fracture Mechanics

journal homepage: www.elsevier.com/locate/tafmec

Stress-intensity factor solutions for embedded elliptical cracks in round bars subjected to tensile load

J.M. Alegre, I.I. Cuesta, A. Díaz *

Grupo de Integridad Estructural, Universidad de Burgos, Escuela Politécnica Superior, Av Cantabria s/n, 09006 Burgos, Spain

ARTICLE INFO

Keywords:
Stress-intensity factor (SIF)
Round bar
Embedded elliptical cracks
Fatigue crack growth
Recategorization of flaws
Internal defects
Fisheye

ABSTRACT

In this paper, stress-intensity factor solutions are presented for an embedded elliptical crack in a round bar subjected to tensile load. The stress-intensity factors (SIF) are presented in a tabulated form and were obtained from three-dimensional finite-element analyses of this crack configuration. The solutions provide the stress-intensity factor as a function of three dimensionless parameters representative of the crack size, the crack aspect ratio of the elliptical flaw and its relative position in the cross section. The dimensionless parameters cover ranges that allow most internal flaw shapes in practice to be considered. In order to validate the numerical model developed, some particular cases are compared with solutions of embedded elliptical flaws in different geometries available in the literature. Afterwards, a sequential methodology for fatigue crack growth is presented, including the conditions for the recategorization from the internal elliptical crack to a semi-elliptical surface crack. A comparison of the predicted crack paths with experimental results of fatigue crack propagation initiated from internal defects in round bars is also presented. This experimental validation shows the capability of the proposed SIF solutions for the study of the fatigue crack propagation initiated from internal defects in this geometry.

1. Introduction

There is a large number of applications in which internal defects, such as pores or inclusions, are the main cause of the fatigue cracks initiation in round bars. For example, the current additive manufacturing techniques, increasingly being used for high responsibility components, are linked to the presence of internal defects, which are the main cause of fatigue crack initiation in these components [1–3]. These internal defects grow due to fatigue until they reach the surface of the specimen, forming a characteristic shape known as a *fisheye*. Moreover, several papers show that the inner inclusion induced failure with the existence of a fisheye becomes the predominant failure mode in High Cycle Fatigue (HCF) and Very High Cycle Fatigue (VHCF) regimes [4–6].

Since one of the most common specimens to study the fatigue life of materials is the cyclic uniaxial tensile test, solutions for the stress-intensity factor for embedded elliptical cracks in round bars subjected to tensile loads are needed.

The calculation of stress-intensity factors (SIF) for embedded elliptical cracks in different geometries has received a great deal of attention in the literature over the last decades.

The exact solution for an embedded elliptical crack in an infinite solid subjected to uniform uniaxial stress was first developed by Green [7] and Irwin [8,9]. After that, extensive research has been conducted on the calculation of stress-intensity factors of embedded elliptical cracks in plates. Varfolomeev and Vainshtok [10] developed a solution based on the method of weight functions to solve the SIF for different load cases including uniform, linear and exponential stress distributions. The same authors [11] present a review of the analytical solutions for the stress-intensity factors along the front of part-elliptical cracks (elliptical, semi-elliptical and quarter-elliptical), including an estimation of the average errors. Newman and Raju [12] provide the stress-intensity factor for embedded elliptical, semi-elliptical surface cracks, and quarter-elliptical corner cracks in plates subjected to tensile and bending loads. The stress-intensity factors are collected as closed form equations obtained from three-dimensional finite-element analyses of these crack configurations. Isida and Noguchi [13] also provide a solution for the stress-intensity factor of finite thickness plates under tension containing an embedded elliptical crack located at an arbitrary position. The solutions, based on numerical calculations, are also presented in

* Corresponding author.
E-mail address: adportugal@ubu.es (A. Díaz).

https://doi.org/10.1016/j.tafmec.2021.103189
Received 9 August 2021; Received in revised form 1 October 2021; Accepted 17 November 2021
Available online 20 November 2021

polynomial forms for practical use.

For the case of internal flaws in round bars, there are a great number of papers focused on the study of penny-shaped cracks. Nishioka and Atluri [14] evaluate a round bar with an embedded circular crack located at the center of the bar, and subjected to pure tension or pure bending at the ends of the bar. Benthem *et al* [15] also provide the stress-intensity factor solution for a circular embedded crack (centered) in a round bar, and subjected to tensile, bending and torsion loads. This last solution is given in the FITNET code of practice [16] and in the FKM guideline [17].

For the case of surface flaws in rounded bars under tension and bending, a great amount of research can be found in the literature [18–23]. A critical review of the most commonly used solutions can be found in the work of Toribio *et al* [24]. Existing solutions cover different load cases, including tensile stress, bending and torsion moments or even based on complex stress distributions. Shin and Cai [18] considered a three-parameter model to represent the crack front and provide both tabulated solutions and a set of practical closed-form equations obtained by a least-squares fitting that allow the SIF at any point of the crack front to be obtained.

Carpinteri *et al* [23] have extensively studied this surface crack geometry considering a three-parameter K-solution to represent the crack front as an elliptical-arc shape, and including a detailed and rigorous methodology for addressing crack growth in this geometry. This is especially interesting because of the loss of perpendicularity of the crack front on the surface of the part. Another interesting reference for this type of surface crack in a round bar is provided by Raju and Newman [19].

For this surface crack geometry, most authors replicate the crack shape evolution during fatigue growth from elliptical-arc or circular-arc shapes. Lin and Smith [25] found that the elliptical-arc surface flaw becomes close to the propagation of the crack fronts during a fatigue process. They also demonstrate that the crack growth always attempts to follow a preferred propagation aspect ratio no matter what the initial crack shape was.

Therefore, numerous solutions for obtaining the SIF in cylindrical round bars when considering a surface arc-elliptical crack have been reported in the literature. There are also numerous papers for the calculation of SIF in embedded elliptical cracks in plates. However, only a few solutions of the stress-intensity factor for embedded elliptical cracks in round bars can be found in the literature [14,15,17,26–28], most of them focused on centered penny shaped cracks.

Consequently, the main objective of this paper is to provide a set of SIF solutions for the case of embedded elliptical cracks in a round bar subjected to tensile loads. Moreover, to use the proposed solutions for a fatigue crack growth analysis, a sequential methodology including the procedure for the recategorization of an internal elliptical crack to a semi-elliptical surface crack is also presented. This recategorization from an embedded elliptical flaw to a surface flaw is required in order the fatigue crack propagation to be extended until the critical fracture conditions are reached. As a general rule, procedures for the recategorization of flaws are collected in the main design codes for the case of plates [28–30].

2. Geometry of the embedded crack in the round bar

The geometry of the round bar and the main dimensions of a generic embedded elliptical crack are presented in Fig. 1.

For an elliptical crack shape, the crack position in the cross section and the aspect ratio are defined by three parameters, the two semi-axes of the ellipse (a and c) and the width of the ligament (h). The bar is defined by the radius (R), and the tensile load applied at the ends of the bar is defined by the constant uniaxial stress (σ_0). These geometric parameters have been normalized, defining three new dimensionless parameters that explicitly characterize the flaw shape, size and location. Both the bar radius and the ligament are used to normalize crack size and location, which is a particularity for embedded cracks:

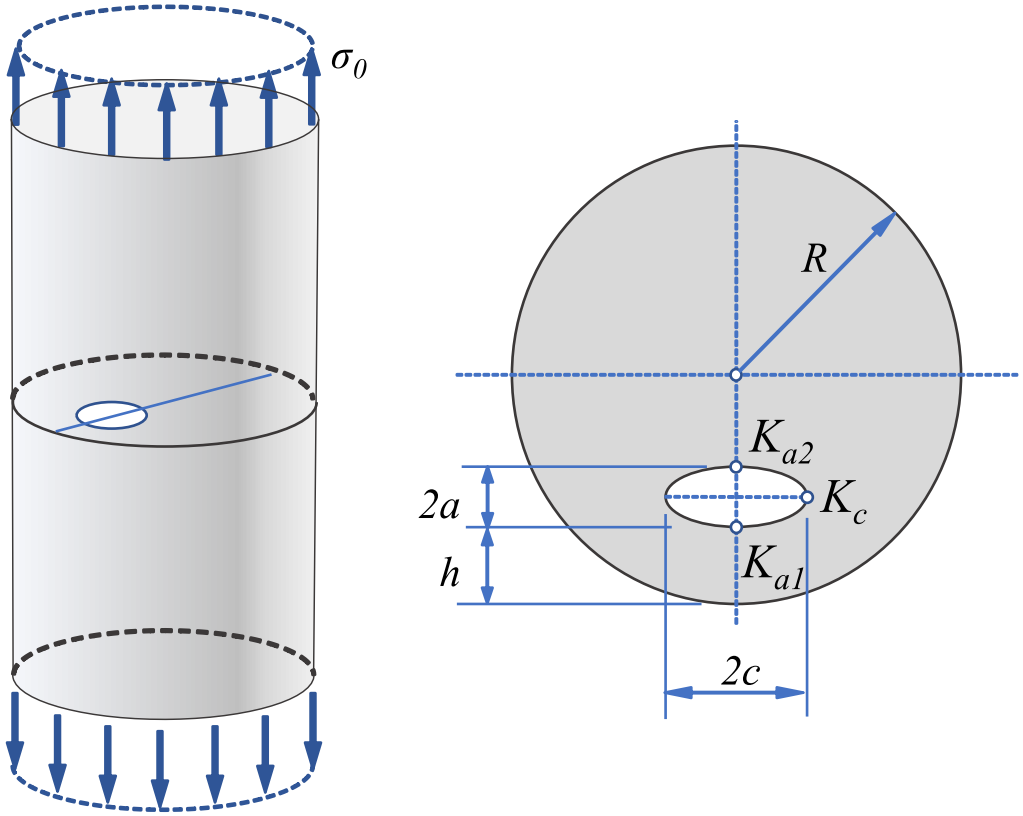

Fig. 1. Dimensions of an embedded elliptical crack in a round bar.

- $(a+h)/R$, which defines the relative position of the center of the crack relative to the center of the circular cross section. This value ranges from 1 for centered cracks to 0.05 for cracks close to the bar surface.
- $a/(a+h)$, which defines the ratio of the crack size to the distance from the center of the ellipse to the bar surface. Its value ranges from 0.05 to 0.95.
- a/c , which defines the aspect ratio of the elliptical crack. Its value ranges from 0.2 for elongated cracks to 1.0 for circular cracks.

The ranges chosen for the dimensionless parameters are based on numerical and practical considerations. The simulated crack aspect ratios and locations do not exhibit mesh distortion or convergence issues. Additionally, the wide range of simulated parameters covers most cases observed in practice for embedded flaws in round bars.

3. Finite element modelling

A numerical 3D model, using Abaqus software, has been created for the SIF calculations using 20-node quadratic elements with reduced integration (C3D20R). The choice of C3D20R is demonstrated to reduce computational time in comparison to C3D20. Nevertheless, for these second-order elements, i.e. quadratic 20-node brick elements, hourglassing is not expected except for very coarse meshes [31], which is not the case in this study. Hourglass modes could appear for linear reduced-integration elements, such as the C3D8R, so they were discarded for this simulation.

Because of its symmetry, only one-fourth of the round bar is modelled. The stress field is determined by assuming a linear elastic behavior with a Poisson ratio of 0.3 and an elastic modulus of 200 GPa. The stress square-root singularity near the flaw is obtained by using quarter-point finite elements around the crack-tip region.

A sensitivity analysis of the mesh size and number of elements along the crack front was performed in order to select the optimum number of elements to balance accuracy and calculation time. A total of 8 elements were chosen to mesh the circular semi-rosette around the tip of the crack, and total of 100 elements were used to mesh the crack front. A detail of the meshing technique used is shown in Fig. 2.

The calculation of the SIF is obtained using the path independent J-integral parameter. This energy-based parameter is implemented in the main finite element analysis codes (e.g. Abaqus) allowing for the calculation of three-dimensional cracks. For elastic–plastic analysis, the J-integral is composed of an elastic part J_e and a plastic part J_p . For linear elastic materials, the elastic part of J-integral, J_e , is related with the stress-intensity factor value, K_I , using the following equation,

$$K_I = \sqrt{J_e \cdot E'} \tag{1}$$

Where $E' = E$ for plane stress and $E' = E/(1-\nu^2)$ for plane strain, with E being Young's modulus and ν Poisson's ratio. Typically, plane strain conditions are assumed along the whole crack front, except at the free surfaces where plane stress conditions can be supposed. In the present study, where an embedded crack is solved, plane strain conditions can be assumed for all points along the crack front.

4. Stress-intensity factor solutions

In order to completely define the SIFs for the elliptical crack, the SIF values at the four vertices of the ellipse need to be obtained. However, because of the symmetry of the crack position (Fig. 1) the values of K_{c1} and K_{c2} are identical, and as a consequence only one value has been calculated and is termed as K_c . On the contrary, the SIFs for the vertices a_1 and a_2 are different because there are placed on a different position in the section and, as a consequence, its values need to be distinguished and calculated. These values are termed as K_{a1} and K_{a2} respectively.

The stress-intensity factor at the vertices of the elliptical crack, as shown in Fig. 1, can be expressed in the following form:

$$\begin{aligned} K_{a1} &= F_{a1} \cdot \sigma_0 \cdot \sqrt{\pi a} \\ K_{a2} &= F_{a2} \cdot \sigma_0 \cdot \sqrt{\pi a} \\ K_c &= F_c \cdot \sigma_0 \cdot \sqrt{\pi a} \end{aligned} \tag{2}$$

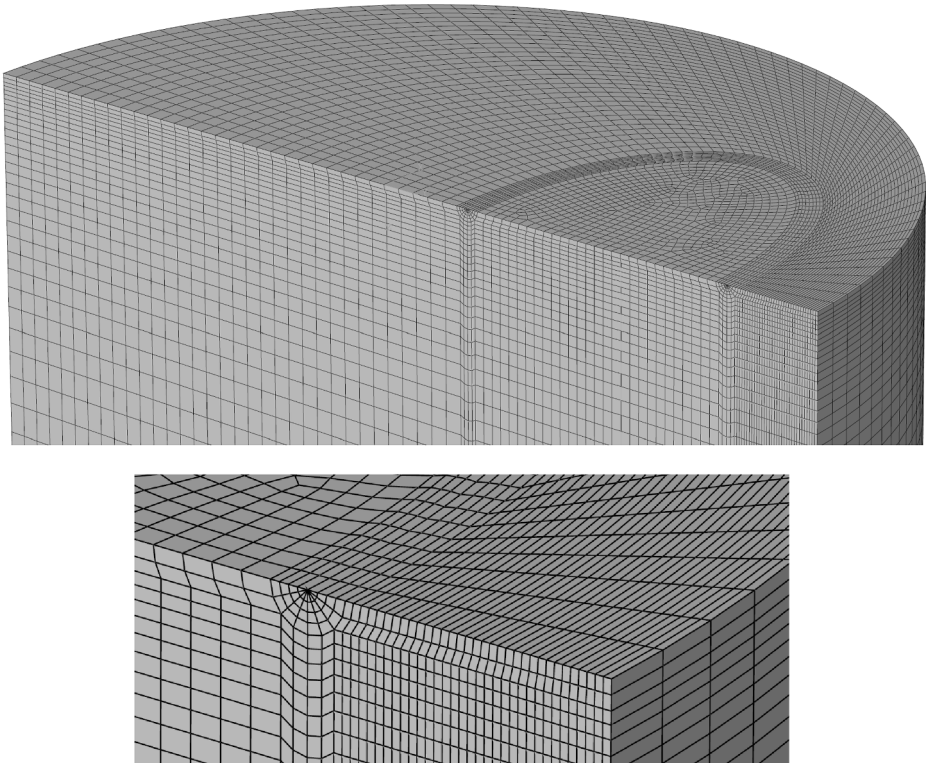

Fig. 2. Detail of the meshing of the numerical model developed for an off-center embedded elliptical crack (a/c = 0.2).

where σ_0 is the uniform axial stress, a is the crack depth, and F_{a1} , F_{a2} and F_c are the geometry correction factors. These factors are a function of crack geometry and the radius of the round bar, and can be written as a function of the three geometric dimensionless parameters in a general form as:

$$F_i = F_i\left(\frac{a+h}{R}, \frac{a}{a+h}, \frac{a}{c}\right) \tag{3}$$

These geometry correction factors are obtained from the 3D numerical calculations of the SIFs presented on Section 3, and then extracted from to equation (2). Tables 1 to 3 collect the calculated values for these geometry correction factors for positions a_1 , a_2 and c respectively. The relative position of the center of the elliptical crack $(a+h)/R$ ranges from 1 (centered crack) to 0.05 (crack close to the bar surface) in six increments 0.05, 0.2, 0.4, 0.6, 0.8 and 1.0. The ratio $a/(a+h)$, which defines the ratio of the crack size to the distance from the crack center to the bar surface, ranges from 0.05 (large ligament size compared to the crack size) to 0.95 (small ligament size compared to the crack size) in six increments. And finally, the aspect ratio of the elliptical crack a/c , ranges from 0.2 (elongated crack) to 1.0 (circular crack) in five equal increments.

5. Comparison with solutions available in the literature

To obtain a suitable finite element model, a comparison of the proposed SIF solutions with others available in the literature is needed. With this aim, two different situations have been analyzed and compared with proven solutions available in the literature.

The first situation analyzed corresponds to a centered circular crack in a round bar subjected to tensile loads. For comparison purpose, the reference solution developed by Benthem *et al* [15] was chosen. This solution is also included in the procedure FITNET [16] and in the guideline FKM [17].

Fig. 3 shows the good agreement of the current SIF results, for the case of $a/(a+h) = 1$ and $a/c = 1$, compared with the solution of Benthem. Only the values for F_{a1} are presented as the values for F_{a2} and F_c are identical for this particular case.

Table 1
Geometry correction factor, F_{a1}.

a/c	$\frac{a}{(a+h)}$	$(a+h)/R$					
		0.05	0.2	0.4	0.6	0.8	1.0
0.2	**0.05**	0.9481	0.9481	0.9481	0.9481	0.9481	0.9481
	0.2	0.9531	0.9543	0.9582	0.9636	0.9695	–
	0.4	0.9834	0.9967	–	–	–	–
	0.6	1.0649	–	–	–	–	–
	0.8	1.2756	–	–	–	–	–
	0.95	1.9484	–	–	–	–	–
0.4	**0.05**	0.8665	0.8665	0.8665	0.8665	0.8665	0.8665
	0.2	0.8689	0.8694	0.8704	0.8722	0.8744	0.8784
	0.4	0.8871	0.8918	0.9068	0.9285	0.9521	–
	0.6	0.9422	0.9635	1.0347	–	–	–
	0.8	1.0790	1.1586	–	–	–	–
	0.95	1.5754	–	–	–	–	–
0.6	**0.05**	0.7812	0.7812	0.7812	0.7812	0.7812	0.7812
	0.2	0.7823	0.7825	0.7828	0.7835	0.7844	0.7862
	0.4	0.7942	0.7966	0.8029	0.8136	0.8250	0.841
	0.6	0.8317	0.8421	0.8753	0.9262	0.9822	–
	0.8	0.9405	0.9765	1.1007	1.3091	–	–
	0.95	1.2667	1.3855	1.8561	–	–	–
0.8	**0.05**	0.7058	0.7058	0.7058	0.7058	0.7058	0.7058
	0.2	0.7067	0.7068	0.7069	0.7072	0.7076	0.7082
	0.4	0.7146	0.7159	0.7191	0.7246	0.731	0.7396
	0.6	0.7413	0.7474	0.7645	0.7927	0.8216	0.8532
	0.8	0.8216	0.8419	0.9063	1.0135	1.1406	–
	0.95	1.0669	1.1293	1.3360	1.7603	–	–
1	**0.05**	0.6386	0.6386	0.6386	0.6386	0.6386	0.6386
	0.2	0.6388	0.6388	0.6389	0.6391	0.6394	0.6398
	0.4	0.6437	0.6446	0.6463	0.6492	0.6529	0.6582
	0.6	0.6631	0.6671	0.6769	0.6936	0.7108	0.7274
	0.8	0.7239	0.7368	0.7731	0.8347	0.8998	0.9525
	0.95	0.9143	0.9520	1.0637	1.2671	1.5391	1.8441

Table 2
Geometry correction factor, F_{a2}.

a/c	$\frac{a}{(a+h)}$	$(a+h)/R$					
		0.05	0.2	0.4	0.6	0.8	1.0
0.2	**0.05**	0.9481	0.9481	0.9481	0.9481	0.9481	0.9481
	0.2	0.9521	0.9531	0.9564	0.9608	0.9663	–
	0.4	0.9692	0.9796	–	–	–	–
	0.6	1.0025	–	–	–	–	–
	0.8	1.0436	–	–	–	–	–
	0.95	1.0870	–	–	–	–	–
0.4	**0.05**	0.8663	0.8663	0.8663	0.8663	0.8663	0.8664
	0.2	0.8679	0.8683	0.8692	0.8705	0.8726	0.8781
	0.4	0.8775	0.8808	0.8917	0.9058	0.9256	–
	0.6	0.8951	0.9101	0.9539	–	–	–
	0.8	0.9214	0.9615	–	–	–	–
	0.95	0.9662	–	–	–	–	–
0.6	**0.05**	0.7804	0.7804	0.7804	0.7804	0.7804	0.7804
	0.2	0.7815	0.7813	0.7816	0.7823	0.7839	0.7866
	0.4	0.7882	0.7897	0.7941	0.7995	0.8102	0.8414
	0.6	0.8001	0.8059	0.8241	0.8499	0.8890	–
	0.8	0.8191	0.8354	0.8915	0.9675	–	–
	0.95	0.8357	0.8698	1.0040	–	–	–
0.8	**0.05**	0.7067	0.7067	0.7067	0.7067	0.7067	0.7067
	0.2	0.7071	0.7071	0.7072	0.7074	0.7078	0.7087
	0.4	0.7104	0.7112	0.7131	0.7163	0.7217	0.7402
	0.6	0.7182	0.7213	0.7306	0.7421	0.7637	0.8538
	0.8	0.7304	0.7385	0.7657	0.8001	0.8611	–
	0.95	0.7409	0.7568	0.8129	0.8929	–	–
1	**0.05**	0.6387	0.6386	0.6386	0.6386	0.6386	0.6386
	0.2	0.6392	0.6392	0.6393	0.6395	0.6398	0.6398
	0.4	0.6409	0.6413	0.6422	0.6439	0.6467	0.6582
	0.6	0.6462	0.6479	0.6527	0.6598	0.6719	0.7274
	0.8	0.6543	0.6589	0.6732	0.6913	0.7237	0.9525
	0.95	0.6584	0.6669	0.6959	0.7296	0.7912	1.8441

Table 3
Geometry correction factor, F_c.

a/c	$\frac{a}{(a+h)}$	$(a+h)/R$					
		0.05	0.2	0.4	0.6	0.8	1.0
0.2	**0.05**	0.4221	0.4221	0.4221	0.4221	0.4221	0.4221
	0.2	0.4236	0.4242	0.4260	0.4291	0.4353	–
	0.4	0.4284	0.4363	–	–	–	–
	0.6	0.4377	–	–	–	–	–
	0.8	0.4545	–	–	–	–	–
	0.95	0.4720	–	–	–	–	–
0.4	**0.05**	0.5477	0.5476	0.5478	0.5478	0.5478	0.5479
	0.2	0.5489	0.5492	0.5499	0.5510	0.5525	0.5559
	0.4	0.5550	0.5578	0.5669	0.5816	0.6100	–
	0.6	0.5666	0.5789	0.6281	–	–	–
	0.8	0.5833	0.6221	–	–	–	–
	0.95	0.6009	–	–	–	–	–
0.6	**0.05**	0.6057	0.6055	0.6057	0.6057	0.6058	0.6058
	0.2	0.6064	0.6065	0.6068	0.6072	0.6079	0.6098
	0.4	0.6120	0.6135	0.6179	0.6252	0.6349	0.6582
	0.6	0.6235	0.6299	0.6514	0.6870	0.7529	–
	0.8	0.6429	0.6624	0.7376	0.9221	–	–
	0.95	0.6567	0.7067	0.9238	–	–	–
0.8	**0.05**	0.6314	0.6314	0.6315	0.6315	0.6315	0.6315
	0.2	0.6318	0.6319	0.6320	0.6322	0.6325	0.6333
	0.4	0.6360	0.6370	0.6393	0.6434	0.6492	0.6623
	0.6	0.6464	0.6504	0.6623	0.6820	0.7090	0.7793
	0.8	0.6642	0.6756	0.7153	0.7835	0.9081	–
	0.95	0.6798	0.7099	0.8018	1.0052	–	–
1	**0.05**	0.6386	0.6386	0.6386	0.6386	0.6386	0.6386
	0.2	0.6389	0.6389	0.6390	0.6392	0.6395	0.6398
	0.4	0.6417	0.6423	0.6436	0.6459	0.6495	0.6582
	0.6	0.6504	0.6531	0.6602	0.6725	0.6889	0.7274
	0.8	0.6660	0.6736	0.6972	0.7367	0.7926	0.9525
	0.95	0.6861	0.6965	0.7487	0.8423	1.0031	1.8441

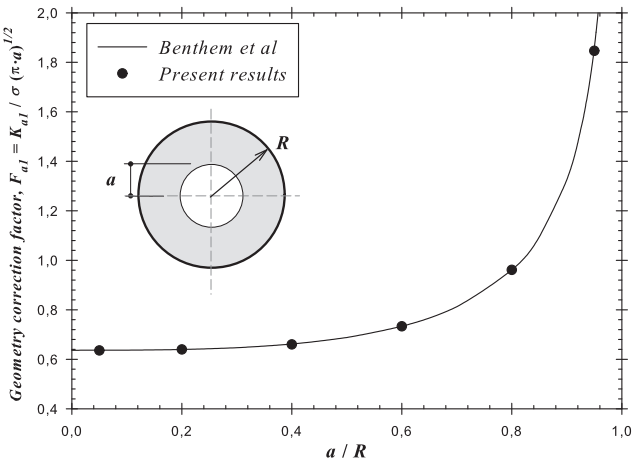

Fig. 3. Comparison of the current solution with the results of Banthem et al [15].

The second situation used for the validation of the present SIF solutions considers an embedded elliptical crack, situated near the bar surface, and sufficiently small compared to the radius of the bar. This particular case agrees with a value of $(a+h)/R = 0.05$, allowing the first column of Tables 1–3 to be verified.

For this particular case, the SIF values are comparable with those corresponding to an embedded elliptical crack on a plate, situated near the plate surface, and also sufficiently small compared to the thickness of the plate. The reference solution on a plate can be taken from Varfolomeev and Vainshtok [10], which is also included as a reference solution in the FKM guideline [17].

Moreover, the solution for an embedded crack in a plate included in the NASGRO software [32] has been also used for the comparison of this second particular case. This crack geometry included in NASGRO, termed as EC04, is a bivariant weight function solution that has improved solution limits making it possible to solve cracks situated very near the plate surface [32].

Figs. 4 to 6 shows the good agreement obtained with this solution for the three geometry correction factors F_{a1} , F_{a2} and F_c . Although the Varfolomeev's solution is limited up to values $a/(a+h) < 0.8$, the improved NASGRO solution (EC4) can be extended up to $a/(a+h) < 1$. In this sense, a very good agreement is observed between present results and the NASGRO solution (EC04) for values up to $a/(a+h) = 0.95$.

Therefore, it can be assumed that the finite element results presented in this paper allow for an accurate SIF calculation within the fixed limits.

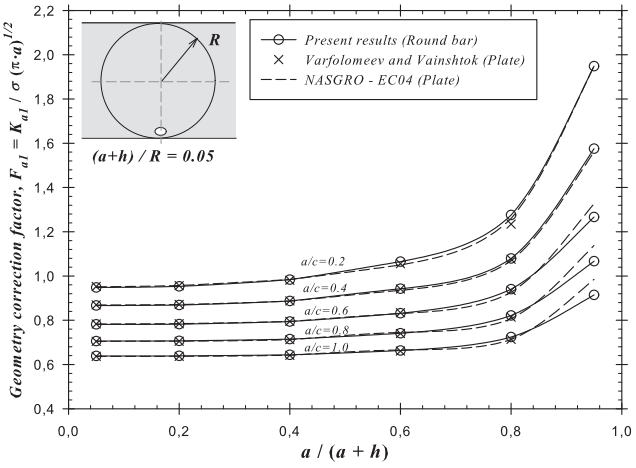

Fig. 4. Comparison of the F_{a1} geometry correction factor for $(a+h)/R = 0.05$, with the Varfolomeev and Vainshtok solution [10].

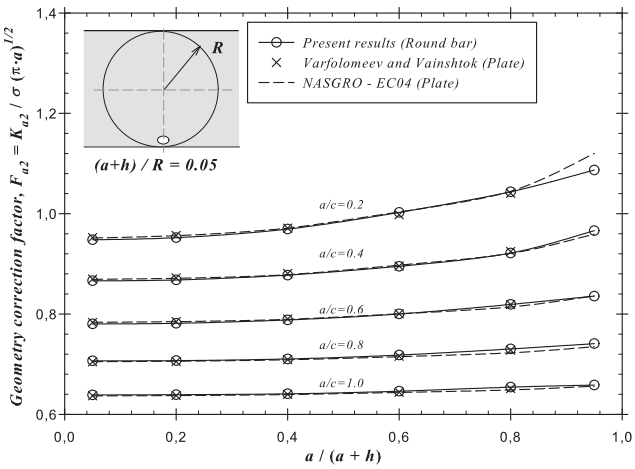

Fig. 5. Comparison of the F_{a2} geometry correction factor for $(a+h)/R = 0.05$, with the Varfolomeev and Vainshtok solution [10].

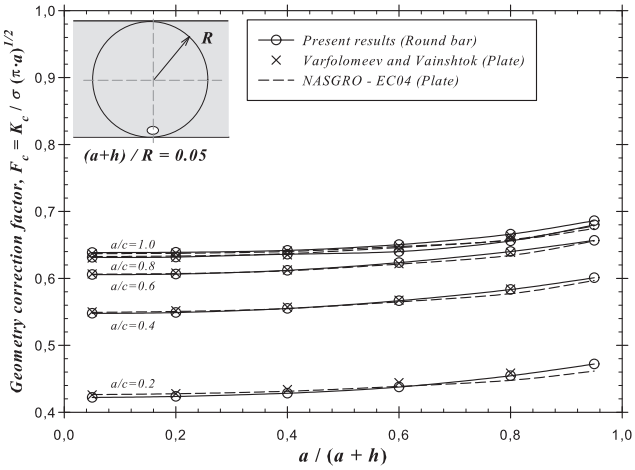

Fig. 6. Comparison of the F_c geometry correction factor for $(a+h)/R = 0.05$, with the Varfolomeev and Vainshtok solution [10].

6. Fatigue crack propagation initiated from internal defects

In order to use the proposed solutions for fatigue crack growth analysis, a sequential methodology is presented in following paragraphs. The crack shape evolution is continuously updated assuming an elliptical crack shape during propagation, using for that the SIF values at the vertices of the elliptical crack. A similar procedure can be found in a paper of Lin and Smith [25] or in a paper of Carpinteri *et al* [23].

The sequential methodology for fatigue crack propagation starts by assuming an initial flaw size and position defined by the three crack parameters ($2a$, $2c$, h). Using these values, three dimensionless geometry parameters, $(a+h)/R$, $a/(a+h)$ and a/c are calculated. Then, the geometry correction factors at the vertices of the ellipse (F_{a1} , F_{a2} and F_c) are obtained using interpolated values collected from Tables 1–3.

For a particular fatigue stress cycle $\Delta\sigma$, the stress-intensity factor ranges at the vertices of the elliptical crack are obtained as:

$$\begin{aligned} \Delta K_{a1} &= F_{a1} \cdot \Delta\sigma \cdot \sqrt{\pi a} \\ \Delta K_{a2} &= F_{a2} \cdot \Delta\sigma \cdot \sqrt{\pi a} \\ \Delta K_{c} &= F_{c} \cdot \Delta\sigma \cdot \sqrt{\pi a} \end{aligned} \tag{4}$$

Once these SIFs are obtained, an appropriate fatigue crack growth law can be employed to obtain the local increments, Δa_1 , Δa_2 and Δc . If a Paris type fatigue crack growth law is applied, $da/dN = C \cdot \Delta K^n$, the new positions of these vertices can be obtained after a user-defined block

of cycles, ΔN , by means of:

$$\begin{aligned}\Delta a_1 &= \Delta N{\cdot}C{\cdot}(\Delta K_{a1})^n \\ \Delta a_2 &= \Delta N{\cdot}C{\cdot}(\Delta K_{a2})^n \\ \Delta c &= \Delta N{\cdot}C{\cdot}(\Delta K_c)^n\end{aligned} \tag{5}$$

The number of cycles selected for the control block (ΔN) should be chosen accordingly to produce sufficiently small crack propagation at every integration step. For this purpose, the expected number of cycles (N) should be divided equally into a large number of blocks. The optimum integration step for a numerical integration is not a fixed value, and its effect on results should be evaluated. For example, a value of $\Delta N = 1000$ *cycles* could be a good initial block size, for expected lives about $2{\cdot}10^5$ cycles, achieving then a number of integration steps about 200. After this first approach, the analyst should evaluate the effect of the integration step size, by reducing or increasing this value, until a small effect on the number of cycles is observed.

Finally, the new crack size and crack positions are redefined according to the following relationships:

$$\begin{aligned}2a_{new} &= 2a + (\Delta a_1 + \Delta a_2) \\ 2c_{new} &= 2c + 2\Delta c \\ h_{new} &= h - \Delta a_1\end{aligned} \tag{6}$$

These steps are repeated, updating the crack shape for each block of cycles, until the failure condition is reached or the desired number of cycles is completed. Failure conditions can be defined in different ways, such us a critical crack size, a critical ligament size or a critical stress-intensity factor value in the vertices of the elliptical crack. This sequential methodology needs to be automated in a computer code to make it possible to solve the fatigue crack growth evolution for a large number of blocks.

An example of the application of the sequential methodology, using the present SIF solutions for two different initial crack aspects ($a/c = 1$ and $a/c = 0.2$) is presented Fig. 7. The initial crack position considered in the example is defined by $(a+h) = 0.6{\cdot}R$. It is interesting to note that a typical feature on this round bar geometry subjected to tensile load is the fact that the internal flaw quickly develops from its initial elliptical shape to a preferred circular shape known as *fisheye*.

Fig. 8 show, as an example, the crack aspect ratio evolution for an initial crack position $(a+h) = 0.6{\cdot}R$, and for three different initial crack aspects. The crack aspect ratio is represented versus the dimensionless parameter $a/(a+h)$, which value ranges from a lower limit close to zero

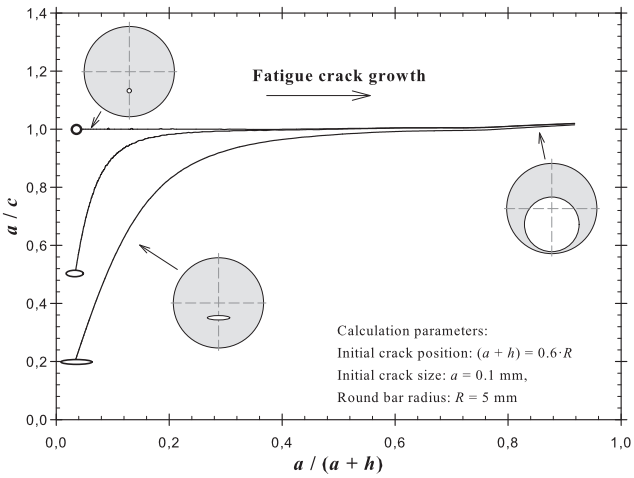

Fig. 8. Fatigue crack shape evolution from three different initial crack aspect ratios (a/c = 1, a/c = 0.5 and a/c = 0.2).

for an initial small crack ($a \ll h$) to a value of $a/(a+h) = 1$ when crack grows and approaches to the surface ($h \to 0$). As can be observed, the initial crack tends quickly to stabilize like a circular crack aspect.

This preferred circular shape during fatigue propagation is also corroborated by experimental fatigue tests carried out on this geometry. Fig. 9 shows an example of the agreement obtained by applying the proposed SIF solutions for the prediction of the crack paths for a uniaxial fatigue test in a round bar. The material is a Ti6Al4V alloy fabricated by selective laser melting (SLM). The fatigue crack growth law is defined in this case using a Paris equation with material parameters $C = 2.99{\cdot}10^{-8}$ and exponent $m = 2.9$ (units in *mm/cycle* and $MPa{\cdot}m^{1/2}$) [33].

7. Recategorization of an embedded crack in a round bar

In some cases, especially for moderate loads, the specimen failure occurs before the fatigue crack reaches the surface of the bar. But in other cases, during fatigue growth of an internal defect, the remaining ligament becomes progressively thinner until it breaks due plastic collapse. This failure of the ligament is not always critical to the overall integrity of the component, and, in such cases, the crack may continue

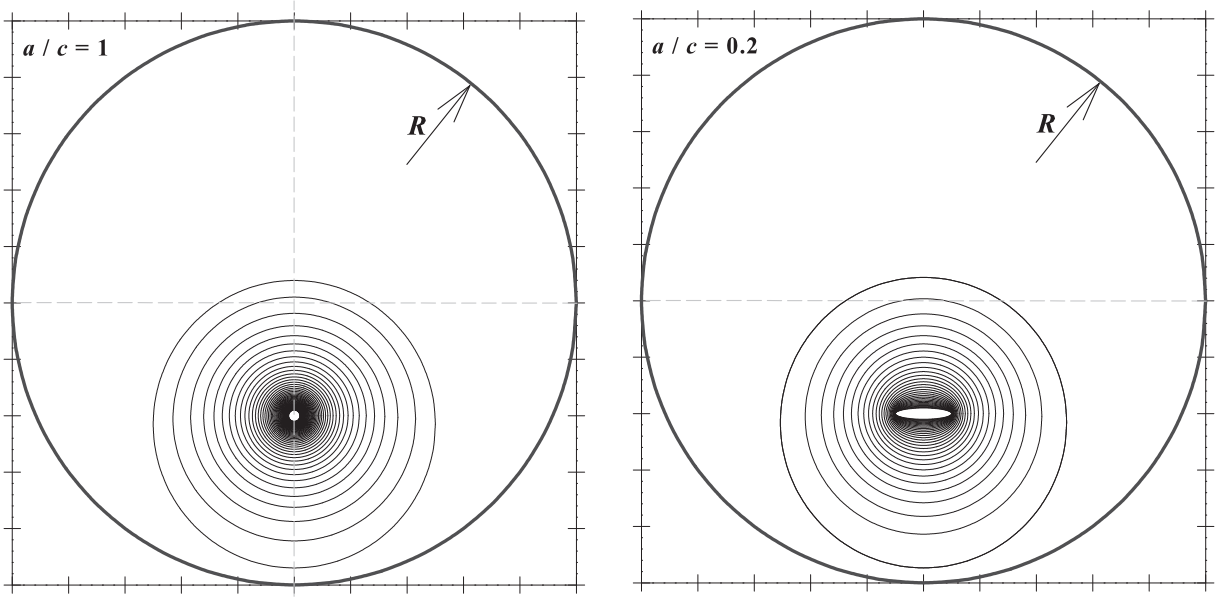

Fig. 7. Examples of fatigue crack path predicted for two different initial crack aspect ratios (a/c = 1 and a/c = 0.2).

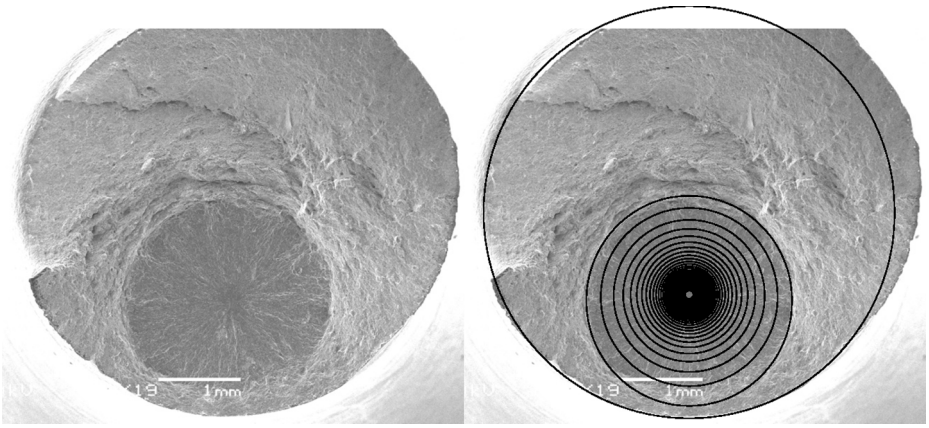

Fig. 9. Experimental and predicted fatigue crack paths initiated from an internal defect on a round bar subjected to fatigue tensile load.

its fatigue growth once the internal defect becomes a surface crack. The recategorization from an internal crack to a surface cracks has been extensively studied in the case of plates and some recommendations are contained in major design codes such as BS 7910 [30].

For the recategorization of an embedded crack to a surface crack in a round bar, an analogous approach to that used for plates in BS 7910 can be assumed, as shown in Fig. 10. In this sense, an embedded crack of size ($2c_e$, $2a_e$) with a remaining ligament of size h, can be recategorized to a surface crack of size

$$\begin{aligned} a_s &= 2a_e + h \\ 2c_s &= 2a_e + 2c_e + h \end{aligned} \tag{7}$$

Where a_s and $2c_s$ are the length and depth of the surface flaw respectively. The transition of an embedded crack to a surface crack is effected instantaneously in a fatigue analysis, and consequently the number of cycles for this transition is not taking into account for the fatigue life of the component.

Fig. 11 shows an example of the propagation of an embedded flaw that grows until reaches the surface and continues growing as a surface crack until failure conditions are reached. As can be observed, the proposed recategorization rule allows for a correct transition from the embedded to surface crack.

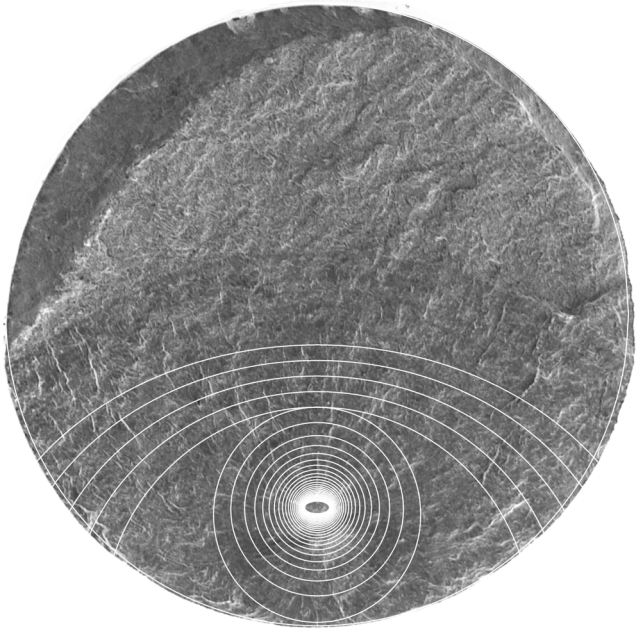

Fig. 11. Fatigue crack growth propagation with recategorization from an embedded crack to a surface crack (fractography courtesy of Niendorf [5]).

8. Conclusions

This paper presents a set of new solutions for the SIF calculation at the vertices of the elliptical embedded cracks in round bars subjected to tensile loads. The geometry correction factors are presented in a tabulated form as a function of three dimensionless parameters

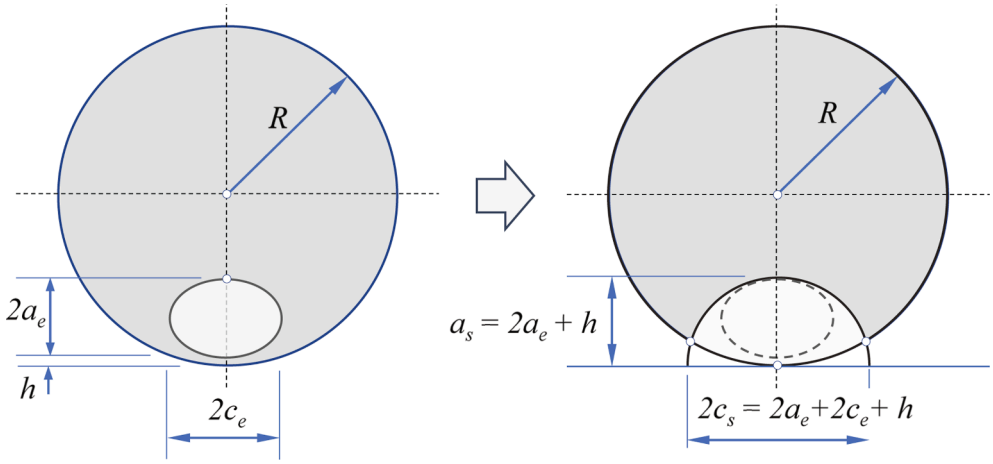

Fig. 10. Procedure for the recategorization from an embedded crack to a surface crack.

representative of the crack and geometry. A comparison of the proposed SIF solutions with others particular cases available in the literature has been carried out, and a very good agreement is obtained.

In order to apply the present SIF solutions for the simulation of the fatigue crack growth a proven and consistent methodology is used. This methodology allows the crack shape evolution to be updated during fatigue process, assuming an elliptical crack shape evolution during propagation.

For this round bar geometry subjected to uniaxial fatigue loads, a preferred circular shape during fatigue propagation is obtained when the crack is initiated from internal defects. In this way, the typical fisheye shape generated during fatigue crack growth, characteristic of VHCF and HCF, can be adequately simulated using the present SIF solutions. A good agreement is also obtained between the numerical analysis, using present SIF solutions, and some experimental fatigue tests.

In those cases where the flaw is close to the surface, the solutions provided make it possible to study the embedded crack growth until reaches the geometry surface. From this point on, a recategorization of the embedded crack to a surface crack is proposed, which is adapted from the procedure for crack recategorization in plates included in the BS 7910 design code.

In this way, the SIF solutions provided in this paper for embedded elliptical cracks can be extended by using other existing solutions for surface elliptical-arc cracks (e.g. Shin and Cai) allowing for a complete study of the fatigue crack growth on round bars subjected to tensile loads initiated from embedded pores or defects.

CRediT authorship contribution statement

J.M. Alegre: Conceptualization, Methodology, Investigation, Data curation, Validation, Visualization, Writing – original draft, Supervision. **I.I. Cuesta:** Conceptualization, Investigation, Data curation, Software, Formal analysis. **A. Díaz:** Investigation, Formal analysis, Writing – review & editing.

Declaration of Competing Interest

The authors declare that they have no known competing financial interests or personal relationships that could have appeared to influence the work reported in this paper.

Acknowledgments

The authors wish to acknowledge the funding received through the JCyL project reference BU-002-P20, co-financed with FEDER funds.

References

[1] Y.N. Hu, S.C. Wu, P.J. Withers, J. Zhang, H.Y.X. Bao, Y.N. Fu, G.Z. Kang, The effect of manufacturing defects on the fatigue life of selective laser melted Ti-6Al-4V structures, Mater. Des. 192 (2020) 108708, https://doi.org/10.1016/j.matdes.2020.108708.

[2] M. Benedetti, V. Fontanari, M. Bandini, F. Zanini, S. Carmignato, Low- and high-cycle fatigue resistance of Ti-6Al-4V ELI additively manufactured via selective laser melting: Mean stress and defect sensitivity, Int. J. Fatigue. 107 (2018) 96–109, https://doi.org/10.1016/j.ijfatigue.2017.10.021.

[3] M. Kahlin, H. Ansell, J.J. Moverare, Fatigue behaviour of notched additive manufactured Ti6Al4V with as-built surfaces, Int. J. Fatigue. 101 (2017) 51–60, https://doi.org/10.1016/j.ijfatigue.2017.04.009.

[4] Z. Sun, W. Li, H. Deng, Z. Zhang, Fisheye failure analysis and life design approach for case-carburized gear steel based on statistical evaluation of defect size, Eng. Fail. Anal. 59 (2016) 28–40, https://doi.org/10.1016/j.engfailanal.2015.11.017.

[5] J. Günther, D. Krewerth, T. Lippmann, S. Leuders, T. Tröster, A. Weidner, H. Biermann, T. Niendorf, Fatigue life of additively manufactured Ti–6Al–4V in the very high cycle fatigue regime, Int. J. Fatigue. 94 (2017) 236–245, https://doi.org/10.1016/j.ijfatigue.2016.05.018.

[6] H.Q. Nguyen, L. Gallimard, C. Bathias, Numerical simulation of fish-eye fatigue crack growth in very high cycle fatigue, Eng. Fract. Mech. 135 (2015) 81–93, https://doi.org/10.1016/j.engfracmech.2015.01.010.

[7] A.E. Green, I.N. Sneddon, The distribution of stress in the neighbourhood of a flat elliptical crack in an elastic solid, Math. Proc. Cambridge Philos. Soc. 46 (1) (1950) 159–163, https://doi.org/10.1017/S0305004100025585.

[8] G.R. Irwin, Crack-extension force for a part-through crack in a plate, J. Appl. Mech. Trans. ASME. (1960). DOI: 10.1115/1.3640649.

[9] I.G.R. Tada H., Paris P.C., The Stress Analysis of Cracks Handbook, 3rd ed., Del Research Corporation, Hellertown, 1973.

[10] I. V Varfolomeev, V.A. Vainshtok, Calculation of stress intensity factors of embedded cracks in structural elements, Strength Mater. 20 (1988) 575–582. DOI: 10.1007/BF01528542.

[11] V.A. Vainshtok, I.V. Varfolomeyev, Stress intensity factor equations for part-elliptical cracks and their verification, Eng. Fract. Mech. 34 (1) (1989) 125–136, https://doi.org/10.1016/0013-7944(89)90246-4.

[12] J.C. Newman, I.S. Raju, Stress-intensity factor equations for cracks in three-dimensional finite bodies subjected to tension and bending loads, NASA Tech. Memo. 85793, Lengley Res. Center, Hamton, VA. (1984). https://ntrs.nasa.gov/archive/nasa/casi.ntrs.nasa.gov/19840015857.pdf.

[13] M. Isida, H. Noguchi, Tension of a plate containing an embedded elliptical crack, Eng. Fract. Mech. 20 (3) (1984) 387–408, https://doi.org/10.1016/0013-7944(84)90046-8.

[14] T. Nishioka, S.N. Atluri, Analytical solution for embedded elliptical cracks, and finite element alternating method for elliptical surface cracks, subjected to arbitrary loadings, Eng. Fract. Mech. 17 (3) (1983) 247–268, https://doi.org/10.1016/0013-7944(83)90032-2.

[15] J.P. Benthem, W.T. Koiter, Asymptotic approximations to crack problems, Methods Anal. Solut. Crack Probl. (1973), https://doi.org/10.1007/978-94-017-2260-5_3.

[16] M. Kocak, S. Webster, J.J. Janosch, R.A. Ainsworth, R. Koers, FITNET Fitness-for-Service (FFS) Procedure, 2008.

[17] B. Pyttel, I. Varfolomeyev, C. Berger, FKM-guideline "fracture mechanics proof of strength for engineering components", Materwiss. Werksttech. (2007) https://doi.org/10.1002/mawe.200700134.

[18] C.S. Shin, C.Q. Cai, Experimental and finite element analyses on stress intensity factors of an elliptical surface crack in a circular shaft under tension and bending, Int. J. Fract. 129 (3) (2004) 239–264, https://doi.org/10.1023/B:FRAC.0000047784.23236.7d.

[19] I.S. Raju, J.C. Newman, Stress-intensity factors for circumferential surface cracks in pipes and rods under tension and bending loads, ASTM Spec. Tech. Publ. (1986), https://doi.org/10.1520/stp17428s.

[20] M.A. Astiz, An incompatible singular elastic element for two- and three-dimensional crack problems, Int. J. Fract. 31 (1986) 105–124. DOI: 10.1007/BF00018917.

[21] Andrea Carpinteri, Elliptical-Arc Surface Cracks in Round Bars, Fatigue Fract. Eng. Mater. Struct. 15 (11) (1992) 1141–1153, https://doi.org/10.1111/ffe.1992.15.issue-1110.1111/j.1460-2695.1992.tb00039.x.

[22] N. Couroneau, J. Royer, Simplified model for the fatigue growth analysis of surface cracks in round bars under mode I, Int. J. Fatigue. 20 (10) (1998) 711–718.

[23] Andrea Carpinteri, Roberto Brighenti, Fatigue propagation of surface flaws in round bars: A three-parameter theoretical model, Fatigue Fract. Eng. Mater. Struct. 19 (12) (1996) 1471–1480, https://doi.org/10.1111/ffe.1996.19.issue-1210.1111/j.1460-2695.1996.tb00182.x.

[24] J. Toribio, N. Álvarez, B. González, J.C. Matos, A critical review of stress intensity factor solutions for surface cracks in round bars subjected to tension loading, Eng. Fail. Anal. 16 (3) (2009) 794–809, https://doi.org/10.1016/j.engfailanal.2008.06.023.

[25] X.B. Lin, R.A. Smith, Shape growth simulation of surface cracks in tension fatigued round bars, Int. J. Fatigue. 19 (6) (1997) 461–469, https://doi.org/10.1016/S0142-1123(97)00012-1.

[26] I.N. Sneddon, R.J. Tait, The effect of a penny-shaped crack on the distribution of stress in a long circular cylinder, Int. J. Eng. Sci. 1 (3) (1963) 391–409, https://doi.org/10.1016/0020-7225(63)90016-8.

[27] M. Shariati, M.M. Rokhi, H. Rayegan, Investigation of stress intensity factor for internal cracks in FG cylinders under static and dynamic loading, Frat. Ed Integrita Strutt. 11 (2017) 166–180, https://doi.org/10.3221/IGF-ESIS.39.17.

[28] ASME-API, Fitness-for-Service API 579-1/ASME FFS-1, (2016).

[29] B. Bezensek, J.W. Hancock, The re-characterisation of complex defects Part I: Fatigue and ductile tearing, Eng. Fract. Mech. 71 (7-8) (2004) 981–1000, https://doi.org/10.1016/S0013-7944(03)00155-3.

[30] BSI, BS 7910: Guide to methods for assessing the acceptability of flaws in metallic structures, BSI Stand. Publ. (2015).

[31] E.Q. Sun, Shear locking and hourglassing in MSC Nastran, ABAQUS, and ANSYS, in, Msc Softw. Users Meet. (2006) 1–9.

[32] Southwest Research Institute, NASGRO 9.2: Fracture Mechanics and Fatigue Crack Growth Analysis. Software Reference Manual, (2020). www.nasgro.swri.org.

[33] Z.H. Jiao, R.D. Xu, H.C. Yu, X.R. Wu, Evaluation on Tensile and Fatigue Crack Growth Performances of Ti6Al4V Alloy Produced by Selective Laser Melting, Procedia Struct. Integr. 7 (2017) 124–132, https://doi.org/10.1016/j.prostr.2017.11.069.